

Pseudodiffusive transmission of nodal Dirac fermions through a clean d -wave superconductor

J. K. Asbóth, A. R. Akhmerov, A. C. Berceanu, and C. W. J. Beenakker
Instituut-Lorentz, Universiteit Leiden, P.O. Box 9506, 2300 RA Leiden, The Netherlands
 (Dated: September 2009)

We calculate the transmission of electrons and holes between two normal-metal electrodes (N), separated over a distance L by an impurity-free superconductor (S) with d -wave symmetry of the order parameter. Nodal lines of vanishing excitation gap form ballistic conduction channels for coupled electron-hole excitations, described by an anisotropic two-dimensional Dirac equation. We find that the transmitted electrical and thermal currents, at zero energy, both have the pseudodiffusive $1/L$ scaling characteristic of massless Dirac fermions — regardless of the presence of tunnel barriers at the NS interfaces. Tunnel barriers reduce the slope of the $1/L$ scaling in the case of the electrical current, while leaving the thermal current unaffected.

PACS numbers: 74.45.+c, 71.10.Pm, 73.23.-b, 74.72.-h

I. INTRODUCTION

Pseudodiffusive transmission refers to the $1/L$ scaling of the electrical current transmitted over a distance L through a clean sheet of undoped graphene [1]. The same $1/L$ scaling characterizes diffusion in a random potential, but now it applies in the absence of any disorder. There is a large number of theoretical [2–12] and experimental [13–15] studies of this phenomenon, which is understood as a general property of massless Dirac fermions in the limit of vanishing excitation energy. The optical analogue in a photonic crystal with a Dirac spectrum has been studied as well [16–19].

Layered superconductors with a d -wave symmetry of the order parameter (notably the high- T_c cuprates [20]) form an altogether different system in which massless Dirac fermions are known to exist [21–23]. These are so-called nodal fermions, located in the two-dimensional Brillouin zone near the intersections (nodal points) of the Fermi surface with lines (nodal lines) of vanishing excitation gap. Elastic mean free paths l as large as $4\ \mu\text{m}$ have been reached in $\text{YBa}_2\text{Cu}_3\text{O}_{7-\epsilon}$ single-crystals [24], much larger than the superconducting coherence length $\xi_0 \simeq 2\ \text{nm}$. It is the purpose of this work to demonstrate theoretically the pseudodiffusive $1/L$ scaling of the transmission through a d -wave superconductor over the range of lengths between ξ_0 and l . This anomalous scaling was not noticed in earlier studies of similar systems [25–27].

The problem is interesting from a conceptual point of view, because it highlights both the differences and similarities between Dirac fermions produced by a bandstructure (as in graphene or photonic crystals) or produced by a d -wave order parameter. In undoped graphene, the transmitted electrical current I in response to a voltage difference V scales as [2, 3]

$$I = \frac{4e^2}{h} V \frac{W}{\pi L}. \quad (1.1)$$

The length L over which the current is transmitted should be large compared to the Fermi wave length λ_F in

the metal contacts, but small compared to the mean free path l . The length L should also be small compared to the transverse width W of the graphene sheet (to avoid edge effects). Potential barriers (smooth on the scale of the lattice constant) at the interfaces between the metal contacts and the graphene sheet have no effect on the current, because of the phenomenon of Klein tunneling [10].

For the d -wave superconductor, we find a transmitted electrical current per layer equal to

$$I = \frac{2e^2}{h} V \frac{W}{\pi L} \frac{v_F^2 + v_\Delta^2}{v_F v_\Delta} \frac{\Gamma_1}{(2 - \Gamma_1)} \frac{\Gamma_2}{(2 - \Gamma_2)}, \quad (1.2)$$

for $\xi_0 \ll L \ll l, W$. Here $\Gamma_{1,2} \in (0, 1)$ are the tunnel probabilities through the potential barriers at the two normal-metal–superconductor (NS) interfaces. The Dirac equation for nodal fermions is anisotropic [21], with different velocities v_F and v_Δ parallel and perpendicular to the nodal lines. This anisotropy (with $v_F/v_\Delta \approx 15$ in $\text{YBa}_2\text{Cu}_3\text{O}_{7-\epsilon}$) increases the slope of the $1/L$ scaling. Remarkably enough, the anisotropy does not introduce a dependence of the transmitted current on the angle α between the direction of the current and the nodal lines. The result (1.2) holds generically for any orientation, except for a narrow range of angles of order ξ_0/L around $\alpha = 0 \pmod{\pi/4}$.

The tunnel barriers reduce the slope of the $1/L$ scaling of the transmitted electrical current (1.2), by a factor $\Gamma_1\Gamma_2/4$ for small tunnel probabilities. This does not imply that the nodal fermions are only weakly transmitted, but rather that the transmission probabilities for transmission as an electron or as a hole are almost the same for $\Gamma_{1,2} \ll 1$. Indeed, we find that the electrical shot noise power P as well as the transmitted thermal current I_{thermal} (both of which do not depend on the sign of the carriers charge) remain finite in the limit $\Gamma_{1,2} \rightarrow 0$. We interpret this result in terms of a resonant coupling via the nodal lines of the mid-gap states [28, 29] extended along the two NS interfaces. We also find, quite surprisingly, that the thermal conductivity is *independent* of the tunnel probabilities $\Gamma_{1,2}$.

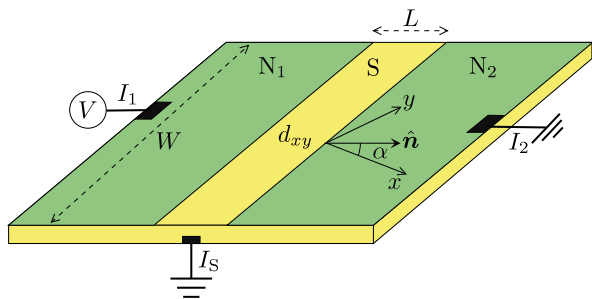


FIG. 1: Geometry to measure the transmission of nodal fermions through a d -wave superconductor. A current I_1 is injected into the superconductor from metal contact N_1 (at a voltage V) and drained to ground via the superconductor (current I_S) or via a second metal contact N_2 (current I_2). If the separation L of the metal contacts is large compared to the superconducting coherence length ξ_0 , the current I_2 is predominantly due to transmission parallel to the nodal lines $x = 0$ or $y = 0$ of vanishing excitation gap .

The outline of this paper is as follows. In Sec. II we formulate the scattering problem and calculate the transfer matrix of the nodal Dirac fermions through the d -wave superconductor. The matching of wave functions at the interface with the metal electrodes is done in Sec. III, both for ideal NS interfaces and for interfaces containing a tunnel barrier. The transmission matrix of electrons and holes follows in Sec. IV. We then apply this result to the calculation of transport properties: the electrical current (Sec. V), the thermal current (Sec. VI), and the electrical shot noise (Sec. VII). We conclude in Sec. VIII with a discussion of our results and an outlook.

II. TRANSFER MATRIX FOR NODAL FERMIONS

A. Anisotropic Dirac equation

We consider a two-dimensional spin-singlet superconductor (S), connecting two normal metal contacts with parallel NS interfaces, separated by a distance L . The transverse dimension W of the superconducting strip (in the x - y plane) is assumed to be large compared to L , in order to avoid edge effects. The order parameter $\Delta(\mathbf{k})$ is assumed to have d_{xy} symmetry: it vanishes for wave vectors along two nodal lines, which are taken to be the x and the y axis. All our results also apply to $d_{x^2-y^2}$ -superconductors, for our purposes, a simple $\pi/4$ rotation relates the two systems. To be specific, the x - y plane can represent a single CuO_2 layer of a cuprate superconductor [20], with the [100] direction at an angle $\pi/4$.

Low-energy excitations in the superconductor are found in the Brillouin zone near the four intersections $(\pm k_F, 0)$, $(0, \pm k_F)$ of the Fermi surface with the nodal lines of the order parameter. (These nodal points are labeled A, B, C, D in Fig. 2.) Around these points, both

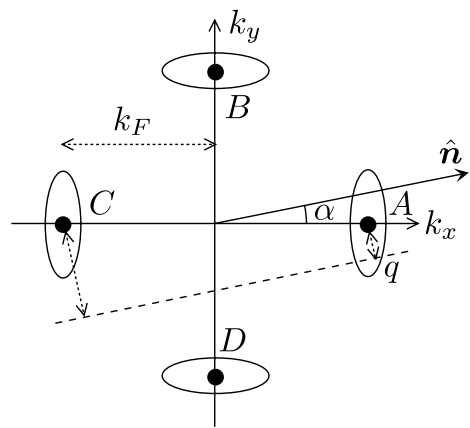


FIG. 2: Ellipsoidal equal-energy contours of low-energy excitations in the Brillouin zone of a superconductor with d_{xy} symmetry. Long and short axes have ratio v_F/v_Δ . The contours are centered at the four nodal points (solid dots), where the order parameter vanishes on the Fermi surface. The normal $\hat{\mathbf{n}}$ to the NS interfaces is indicated. The dashed line, displaced from the nearest nodal point by q , indicates points of constant wave vector component parallel to the interface.

the pair potential $\Delta(\mathbf{k})$ and the kinetic energy can be linearized: the dynamics of the nodal fermions is governed by an anisotropic Dirac equation [21–23]. For example, near node A at $(k_F, 0)$ this can be written in the form

$$\begin{pmatrix} -iv_F\partial_x & -iv_\Delta\partial_y \\ -iv_\Delta\partial_y & iv_F\partial_x \end{pmatrix} \begin{pmatrix} \Psi_e \\ \Psi_h \end{pmatrix} = \varepsilon \begin{pmatrix} \Psi_e \\ \Psi_h \end{pmatrix}, \quad (2.1)$$

or more compactly with the help of Pauli matrices,

$$-i[v_F\sigma_z\partial_x + v_\Delta\sigma_x\partial_y]\Psi = \varepsilon\Psi. \quad (2.2)$$

We have set \hbar to unity, restoring units in the final expressions. The spinor $\Psi = (\Psi_e, \Psi_h)$ contains the envelope wave functions of electron and hole excitations (slowly varying on the scale of the Fermi wavelength $\lambda_F = 2\pi/k_F$). The Fermi velocity v_F is larger than the velocity $v_\Delta = \Delta_0/\hbar k_F$ by a factor of order ξ_0/λ_F (with $\xi_0 = \hbar v_F/\Delta_0$ the superconducting coherence length), which is in the range 10–20 for cuprate superconductors. The equal-energy contours in the Brillouin zone of the nodal fermions thus have an elongated ellipsoidal shape,

$$\varepsilon(\delta\mathbf{k}) = \sqrt{(v_F\delta k_x)^2 + (v_\Delta\delta k_y)^2}, \quad (2.3)$$

as a function of the displacement $\delta\mathbf{k}$ of the wave vector from the nodal point.

B. Transfer matrix

Since the system is translation invariant along the NS interfaces, the component of the wave vector along these interfaces, $q = -\delta k_x \sin \alpha + \delta k_y \cos \alpha$, is a conserved quantity. Here α is the angle between the normal to the NS

interface and the nodal line pointing to node A , which we restrict to $-\pi/4 \leq \alpha \leq \pi/4$ without loss of generality. Moreover, since mirror reflection along the NS interface, followed by the transformation $\Delta(\mathbf{k}) \rightarrow -\Delta(\mathbf{k})$, while leaving all the other parameters unchanged, maps α on $-\alpha$, we can further restrict α to $0 \leq \alpha \leq \pi/4$. In all our formulas, to obtain the corresponding formulas for $-\alpha$, replace q by $-q$ and v_Δ by $-v_\Delta$.

We write $\Psi(\mathbf{r}) = \Psi(s)e^{iqs'}$, with $s \in (0, L)$ the coordinate perpendicular to the NS interfaces and s' the coordinate parallel to them. We substitute $\Psi(\mathbf{r})$ into Eq. (2.1) and find that the spinor $\Psi(s)$ satisfies the wave equation

$$[-iJ\partial_s + J_1q]\Psi(s) = \varepsilon\Psi(s), \quad (2.4)$$

where ∂_s is differentiation perpendicular to the NS interface, and J and J_1 are the operators of particle current perpendicular and parallel to the NS interface,

$$J = v_F\sigma_z \cos \alpha + v_\Delta\sigma_x \sin \alpha, \quad (2.5)$$

$$J_1 = v_\Delta\sigma_x \cos \alpha - v_F\sigma_z \sin \alpha. \quad (2.6)$$

We note that the operator J squares to a scalar, its magnitude giving the particle velocity v_α perpendicular to the NS interface:

$$v_\alpha^2 = J^2 = v_F^2 \cos^2 \alpha + v_\Delta^2 \sin^2 \alpha. \quad (2.7)$$

To solve Eq. (2.4), we multiply it by J/v_α^2 and rearrange to obtain

$$\partial_s\Psi(s) = i\mathcal{A}_0\Psi(s), \quad (2.8)$$

with

$$\mathcal{A}_0 = q \frac{\sin 2\alpha}{2} \frac{v_F^2 - v_\Delta^2}{v_\alpha^2} + \frac{\varepsilon}{v_\alpha^2} J - iq \frac{v_F v_\Delta}{v_\alpha^2} \sigma_y. \quad (2.9)$$

The solution to Eq. (2.4) can then be written as

$$\Psi(s_0 + s) = \mathcal{M}_s\Psi(s_0); \quad \mathcal{M}_s = \exp[i\mathcal{A}_0 s], \quad (2.10)$$

where the second equation defines the *transfer matrix* \mathcal{M}_s . As expected, the particle current J is conserved by Eq. (2.4): $\partial_s [\Psi^\dagger(s)J\Psi(s)] = \Psi^\dagger(s)[-i\mathcal{A}_0^\dagger J + iJ\mathcal{A}_0]\Psi(s) = 0$.

III. WAVE MATCHING AT THE NS INTERFACES

At the two NS interfaces the coupled electron-hole excitations in the superconductor are converted into uncoupled electrons and holes in the normal metal. We thus need to match, at $s = 0$ and $s = L$, the envelope wave functions $\Psi = (\Psi_e, \Psi_h)$ of the nodal fermions in S to the Bloch wave functions $\Phi = (\Phi_e, \Phi_h)$ of free fermions in N. This is similar to the matching of Dirac equation to Helmholtz equation considered in the context of transmission through a photonic crystal [16]. Translational invariance parallel to the NS interfaces requires that the coupling conserve the wave vector component q parallel to the interfaces. Particle flux conservation imposes further constraints, as we determine here.

A. Particle flux conservation at the NS interface

At the surface of the superconductor, the order parameter Δ attains its bulk value over a short length scale, the healing length l_0 . The two-component wave function on the S side of the interface (at $s = l_0$) can be linked to that on the N side ($s = 0$) by an *interface matrix* \mathcal{M}_{NS} , defined by

$$\Psi(l_0) = \mathcal{M}_{NS}\Psi(0). \quad (3.1)$$

In the normal metal, the operator of particle flux perpendicular to the NS interface can be written as

$$j_N = v_N\sigma_z, \quad (3.2)$$

with v_N possibly different from $v_F \cos \alpha$ because of a Fermi energy mismatch. The requirement of particle flux conservation reads

$$\Psi(0)^\dagger v_N\sigma_z\Psi(0) = \Psi(0)^\dagger \mathcal{M}_{NS}^\dagger J \mathcal{M}_{NS}\Psi(0). \quad (3.3)$$

To derive the most general form of the interface matrix fulfilling this requirement, notice that a unitary rotation through angle θ , where

$$\theta = \arctan \left[\frac{v_\Delta}{v_F} \tan \alpha \right], \quad (3.4)$$

transforms J into σ_z up to a scalar factor:

$$v_\alpha\sigma_z = \exp[i\theta\sigma_y/2]J \exp[-i\theta\sigma_y/2]. \quad (3.5)$$

This allows us to write the interface matrix as

$$\mathcal{M}_{NS} = \sqrt{\frac{v_N}{v_\alpha}} \exp[-i\theta\sigma_y/2]\mathcal{M}_0, \quad (3.6)$$

where \mathcal{M}_0 is a 2×2 matrix fulfilling a generalized unitarity condition,

$$M_0^{-1} = \sigma_z M_0^\dagger \sigma_z. \quad (3.7)$$

Eq. (3.7) restricts M_0 to a three-parameter form

$$M_0 = e^{\beta_x\sigma_x} e^{\beta_y\sigma_y} e^{i\beta_z\sigma_z} \quad (3.8)$$

(ignoring an irrelevant scalar phase factor), with arbitrary real parameters $\beta_x, \beta_y, \beta_z$. To understand better where the nontrivial interface matrix arises from, and to show that we may set $\beta_x = \beta_y = \beta_z = 0$, we have to extend the Dirac equation (2.4) to the interface layer, where v_Δ varies in space. This is done in Appendix A.

So far we have considered only *intranode* scattering at the NS interface. We refer to such an interface as an “ideal interface”. A nonideal interface contains a tunnel barrier, which introduces *internode* scattering. We will consider the transfer matrices through the *d*-wave superconductor for both cases in the next two subsections.

B. Transfer matrix with ideal NS interfaces

The complete transfer matrix for a strip of d -wave superconductor with ideal NS interfaces reads

$$\mathcal{M}_{\text{ideal}} = \mathcal{M}_{NS}^{-1} \mathcal{M}_L \mathcal{M}_{NS}, \quad (3.9)$$

where \mathcal{M}_L is the \mathcal{M}_s from Eq. (2.10) with $s = L$, describing propagation inside the superconductor, and \mathcal{M}_{NS} from Eq. (3.6), with $\mathcal{M}_0 = 1$, describes an NS interface. Upon substitution, we obtain

$$\begin{aligned} \mathcal{M}_{\text{ideal}} &= e^{i\phi_\alpha(q)} \exp\left(\frac{iL\varepsilon}{v_\alpha} \sigma_z + qL \frac{v_F v_\Delta}{v_\alpha^2} \sigma_y\right) \\ &= e^{i\phi_\alpha(q)} \left[\cosh[\kappa_\alpha(q)L] \right. \\ &\quad \left. + \frac{\sinh[\kappa_\alpha(q)L]}{v_\alpha^2 \kappa_\alpha(q)} (i\varepsilon v_\alpha \sigma_z + q v_F v_\Delta \sigma_y) \right], \quad (3.10) \end{aligned}$$

with the definitions

$$\kappa_\alpha(q) = \sqrt{(q v_F v_\Delta / v_\alpha^2)^2 - (\varepsilon / v_\alpha)^2}, \quad (3.11)$$

$$\phi_\alpha(q) = qL \frac{v_F^2 - v_\Delta^2}{v_\alpha^2} \frac{\sin 2\alpha}{2}. \quad (3.12)$$

Notice, how – as a result of accounting for the two NS interfaces – the transfer matrix has simplified from that of Eq. (2.10). The change is that the particle flux operator J in Eq. (2.9) is replaced by $v_\alpha \sigma_z$ in Eq. (3.10). Also note that the determinant of the transfer matrix has norm one, $\text{Det} \mathcal{M}_{\text{ideal}} = e^{2i\phi_\alpha(q)}$, as required by the generalized unitarity relation

$$\mathcal{M}^{-1} = \sigma_z \mathcal{M}^\dagger \sigma_z, \quad (3.13)$$

which holds for any transfer matrix as a consequence of particle current conservation.

To appreciate the effects of the Dirac cone anisotropy, we can perform a linear transformation on our system to obtain one with an isotropic Dirac cone: contraction along the nodal line by a factor v_Δ / v_α , and expansion perpendicular to it by a factor v_F / v_α . The dispersion of the new, isotropic Dirac cone has a single velocity parameter $v = v_F v_\Delta / v_\alpha$. The superconducting strip is deformed by the transformation: its width W is unchanged, but its length L becomes

$$L_\alpha = L \frac{v_F v_\Delta}{v_\alpha^2}, \quad (3.14)$$

an effective propagation length we define here for later use.

The matrix (3.10) derived above is the transfer matrix for nodal fermions near point $\mathbf{k}_A = (k_F, 0, 0)$ on the Fermi surface, with $q \equiv q_A = (\mathbf{k} - \mathbf{k}_A) \cdot (\hat{\mathbf{z}} \times \hat{\mathbf{n}})$ the transverse wave vector component relative to k_A . Similarly, the transfer matrices near each of the four nodal points

can be written as

$$\mathcal{M}_A = e^{i\phi_\alpha(q_A)} \exp\left(\frac{iL\varepsilon}{v_\alpha} \sigma_z + \frac{q_A L v_F v_\Delta}{v_\alpha^2} \sigma_y\right), \quad (3.15a)$$

$$\mathcal{M}_B = e^{-i\phi_{\pi/2-\alpha}(q_B)} \exp\left(\frac{iL\varepsilon}{v_{\pi/2-\alpha}} \sigma_z - \frac{q_B L v_F v_\Delta}{v_{\pi/2-\alpha}^2} \sigma_y\right), \quad (3.15b)$$

$$\mathcal{M}_C = e^{i\phi_\alpha(q_C)} \exp\left(-\frac{iL\varepsilon}{v_\alpha} \sigma_z + \frac{q_C L v_F v_\Delta}{v_\alpha^2} \sigma_y\right), \quad (3.15c)$$

$$\mathcal{M}_D = e^{-i\phi_{\pi/2-\alpha}(q_D)} \exp\left(-\frac{iL\varepsilon}{v_{\pi/2-\alpha}} \sigma_z - \frac{q_D L v_F v_\Delta}{v_{\pi/2-\alpha}^2} \sigma_y\right). \quad (3.15d)$$

The basis at each nodal point is the same spinor (Φ_e, Φ_h) , but the electron states Φ_e are “right-movers” (propagating from N_1 to N_2) at nodal points A or B and “left-movers” (from N_2 to N_1) at nodal points C and D .

C. Nonideal interfaces

The complete Fermi surface of the normal metal (N) might differ in many ways from that of the superconductor. However, when we study transport near a specific nodal point, due to transverse momentum conservation, we can effectively reduce the Fermi surface to the two \mathbf{k} points where transverse momentum has the same value as at the nodal point. These two \mathbf{k} points in N each couple to different nodal points in S, for example to nodal points A and C in Fig. 2. A nonideal NS interface couples different nodal points, by reversing the component of the momentum perpendicular to the interface. Such *internode scattering* may be caused by an insulating layer at the NS interface, or it may result from the Fermi velocity mismatch between N and S. Note that only internode scattering is possible in the absence of superconducting order — any *intranode* scattering has to happen inside the superconductor.

We will generically describe a nonideal NS interface by a tunnel barrier, with tunnel probability Γ (which we take mode independent for simplicity). For $|\alpha| \lesssim \xi_0 / L$, the tunnel barrier couples electrons near nodal points A and C . The transfer matrix $\mathcal{M}_\Gamma(s_0)$ for a tunnel barrier at position s_0 , defined by

$$\begin{pmatrix} \Phi_{e,A} \\ \Phi_{e,C} \end{pmatrix}_{s_0^+} = \mathcal{M}_\Gamma(s_0) \begin{pmatrix} \Phi_{e,A} \\ \Phi_{e,C} \end{pmatrix}_{s_0^-}, \quad (3.16)$$

has the form

$$\mathcal{M}_\Gamma(s_0) = \sqrt{\frac{1}{\Gamma}} \begin{pmatrix} 1 & e^{-i\phi(s_0)} \sqrt{1-\Gamma} \\ e^{i\phi(s_0)} \sqrt{1-\Gamma} & 1 \end{pmatrix}, \quad (3.17)$$

with $\phi(s) = 2k_F s \cos \alpha$.

The tunnel barrier at s_0 also couples holes near nodal points A and C , with transfer matrix

$$\begin{pmatrix} \Phi_{h,C} \\ \Phi_{h,A} \end{pmatrix}_{s_0^+} = \mathcal{M}_\Gamma^*(s_0) \begin{pmatrix} \Phi_{h,C} \\ \Phi_{h,A} \end{pmatrix}_{s_0^-}, \quad (3.18)$$

(The basis states are chosen such that the upper component is a right-mover and the lower component a left-mover.)

Finally, we can write down the full transfer matrix of the superconducting strip, in the basis $(\Phi_{e,A}, \Phi_{h,A}, \Phi_{e,C}, \Phi_{h,C})$, including nonideal contacts with tunneling probabilities Γ_1 at $s = 0$ and Γ_2 at $s = L$. It is obtained by matrix multiplication,

$$\mathcal{M} = V \begin{pmatrix} \mathcal{M}_{\Gamma_2}(L) & 0 \\ 0 & \mathcal{M}_{\Gamma_2}^*(L) \end{pmatrix} V^\dagger \begin{pmatrix} \mathcal{M}_A & 0 \\ 0 & \mathcal{M}_C \end{pmatrix} \cdot V \begin{pmatrix} \mathcal{M}_{\Gamma_1}(0) & 0 \\ 0 & \mathcal{M}_{\Gamma_1}^*(0) \end{pmatrix} V^\dagger, \quad (3.19)$$

with V a unitary matrix that switches bases from $(\Phi_{e,A}, \Phi_{e,C}, \Phi_{h,C}, \Phi_{h,A})$ to $(\Phi_{e,A}, \Phi_{h,A}, \Phi_{e,C}, \Phi_{h,C})$:

$$V = \begin{pmatrix} 1 & 0 & 0 & 0 \\ 0 & 0 & 0 & 1 \\ 0 & 1 & 0 & 0 \\ 0 & 0 & 1 & 0 \end{pmatrix}. \quad (3.20)$$

If $\pi/4 - \alpha \lesssim \xi_0/L$, the nodal point A is coupled to the nodal point D , so the above formulas still hold, with C replaced by D .

If both $\alpha \gg \xi_0/L$ and $\pi/4 - \alpha \gg \xi_0/L$, the tunnel barriers at the interfaces do not couple nodal point A to any other nodal points. Since we assume $\xi_0/L \ll 1$, this case of misaligned nodes is the generic case. In that case, \mathcal{M}_C is to be replaced by the singular transfer matrix $\mathcal{M}_{\text{Andreev}}$ corresponding to Andreev reflection with reflection amplitude $-i$,

$$\mathcal{M}_{\text{Andreev}} = \lim_{z \rightarrow \infty} e^{-z\sigma_y}. \quad (3.21)$$

Since $\mathcal{M}_{\text{Andreev}}$ is also the $q_C \rightarrow -\infty$ limit of $\mathcal{M}_C(q_C)$ in Eq. (3.15c) (up to an irrelevant phase factor), Eq. (3.19) is valid as it stands for misaligned nodes as well.

IV. TRANSMISSION AMPLITUDES

A. Ideal interfaces

Referring to the geometry of Fig. 1, a scattering state (for a given value of q) has the form $\Phi(0) = (1, r_{he})$ at the normal side of the left NS interface and $\Phi(L) = (t_{ee}, 0)$ at the normal side of the right NS interface. The complex number r_{he} is the amplitude for Andreev reflection (from electron to hole) and the complex number t_{ee} is

the amplitude for electron transmission. We calculate this transmission amplitude using the relation

$$t_{ee} = ([\mathcal{M}_A^{-1}]_{11})^{-1} = ([\mathcal{M}_A^\dagger]_{11})^{-1}, \quad (4.1)$$

where the first equality follows from $\Phi(0) = \mathcal{M}_A^{-1}\Phi(L)$, and the second equality from particle current conservation, Eq. (3.13).

Substitution of Eq. (3.15a) gives the expression

$$t_{ee} = e^{i\phi_\alpha(q_A)} \left[\cosh[\kappa_\alpha(q_A)L] - \frac{i\varepsilon \sinh[\kappa_\alpha(q_A)L]}{v_\alpha \kappa_\alpha(q_A)} \right]^{-1}. \quad (4.2)$$

B. Nonideal interfaces

For nonideal interfaces we have to consider both the transmission amplitude t_{ee} from electron to electron and the transmission amplitude t_{he} from electron to hole. It is convenient to define the 2×2 transmission matrix

$$t = \begin{pmatrix} t_{ee} & t_{eh} \\ t_{he} & t_{hh} \end{pmatrix}, \quad (4.3)$$

which contains also the transmission amplitudes t_{eh} and t_{hh} from hole to electron and from hole to hole. This matrix t is a 2×2 subblock of the 4×4 unitary scattering matrix S , which we derive in Appendix B.

To obtain t from the 4×4 transfer matrix \mathcal{M} , we make a change of basis from the basis $(\Phi_{e,A}, \Phi_{h,A}, \Phi_{e,C}, \Phi_{h,C})$ used in Eq. (3.19) to a basis $(\Phi_{e,A}, \Phi_{h,C}, \Phi_{e,C}, \Phi_{h,A})$ in which the upper two components are right-movers and the lower two components are left-movers. The change of basis is carried out by the unitary matrix

$$W = \begin{pmatrix} 1 & 0 & 0 & 0 \\ 0 & 0 & 0 & 1 \\ 0 & 0 & 1 & 0 \\ 0 & 1 & 0 & 0 \end{pmatrix}. \quad (4.4)$$

We can then follow the same reasoning as in the previous subsection, to conclude that t is determined by the 2×2 upper-left block X_{11} of $W\mathcal{M}W^\dagger$,

$$X_{11}^\dagger t = 1, \quad (4.5)$$

cf. Eq. (4.1).

Substitution of \mathcal{M} from Eq. (3.19) gives, after some algebra,

$$t^\dagger = \frac{(\Gamma_1\Gamma_2)^{1/2}}{Z} \begin{pmatrix} (\mathcal{M}_C)_{22} + e^{i\phi(L)}(\mathcal{M}_A)_{22}\sqrt{1-\Gamma_1}\sqrt{1-\Gamma_2} & -(\mathcal{M}_A)_{12}\sqrt{1-\Gamma_1} - e^{-i\phi(L)}(\mathcal{M}_C)_{12}\sqrt{1-\Gamma_2} \\ -(\mathcal{M}_C)_{21}\sqrt{1-\Gamma_1} - e^{i\phi(L)}(\mathcal{M}_A)_{21}\sqrt{1-\Gamma_2} & (\mathcal{M}_A)_{11} + e^{-i\phi(L)}(\mathcal{M}_C)_{11}\sqrt{1-\Gamma_1}\sqrt{1-\Gamma_2} \end{pmatrix}, \quad (4.6)$$

$$Z = \sqrt{1-\Gamma_1}\sqrt{1-\Gamma_2} \left(e^{-i\phi(L)}\text{Det } \mathcal{M}_C + e^{i\phi(L)}\text{Det } \mathcal{M}_A \right) + (\mathcal{M}_A)_{11}(\mathcal{M}_C)_{22} \\ + (\mathcal{M}_A)_{22}(\mathcal{M}_C)_{11}(1-\Gamma_1)(1-\Gamma_2) - (\mathcal{M}_A)_{12}(\mathcal{M}_C)_{21}(1-\Gamma_1) - (\mathcal{M}_A)_{21}(\mathcal{M}_C)_{12}(1-\Gamma_2). \quad (4.7)$$

V. ELECTRICAL CURRENT

A. Ideal interfaces

Turning now to observable quantities, we will work in the linear response regime $V \rightarrow 0$, when the transmission amplitudes may be evaluated at the Fermi level ($\varepsilon = 0$).

The current I_2^A (per layer) transmitted into metal contact N_2 through nodal point A is obtained by integrating the transmission probability $|t_{ee}|^2$ over q_A ,

$$I_2^A = G_0 V \frac{W}{2\pi} \int dq_A |t_{ee}|^2. \quad (5.1)$$

(The conductance quantum $G_0 = 2e^2/h$ includes a twofold spin degeneracy.) The integrand decays exponentially for $|q_A| \gg v_\alpha^2/v_F v_\Delta L \simeq (\xi_0/L)k_F$. For $L \gg \xi_0$ the effective integration range is much smaller than k_F and may be extended to $\pm\infty$. Substituting Eq. (4.2) (for $\varepsilon = 0$) we arrive at

$$I_2^A = G_0 V \frac{W}{L} \frac{v_\alpha^2}{\pi v_F v_\Delta}. \quad (5.2)$$

As expected, the conductance of a single nodal point has the same form as that of a single valley in a graphene strip, with L replaced by the effective propagation length L_α of Eq. (3.14).

The current I_2^B transmitted through nodal point B is given by the same formula with v_α replaced by $v_{\alpha-\pi/2}$. Because of the identity

$$v_\alpha^2 + v_{\alpha-\pi/2}^2 = v_F^2 + v_\Delta^2, \quad (5.3)$$

the total current $I_2 = I_2^A + I_2^B$ becomes *independent* of α . The conductivity $\sigma_{\text{ideal}} = (I_2/V)(L/W)$ per layer for the case of ideal NS interfaces is then equal to

$$\sigma_{\text{ideal}} = G_0 \frac{v_F^2 + v_\Delta^2}{\pi v_F v_\Delta}. \quad (5.4)$$

As discussed in Sec. VIII A, Eq. (5.4) differs [by a factor $1 + (v_\Delta/v_F)^2$] from the bulk electrical conductivity of Refs. [21, 22].

B. Nonideal interfaces

For nonideal NS interfaces, tunnel barriers couple the nodal points, and the calculation of the current I_2 becomes more involved. In this Section we treat the generic

case of misaligned nodal points. The case of (perfectly) aligned nodal points is considered in Appendix C.

We first calculate the current through nodal point A . As discussed in Sect. III C, we can substitute \mathcal{M}_C with $\mathcal{M}_{\text{Andreev}}$ of Eq. (3.21), and using Eq. (4.6) we obtain the transmission matrix (at $\varepsilon = 0$)

$$t_A^\dagger = \frac{\sqrt{\Gamma_1\Gamma_2}}{e^{i\phi_\alpha(q_A)}Z_A} \times \begin{pmatrix} 1 & -ie^{-i\phi(L)}\sqrt{1-\Gamma_2} \\ i\sqrt{1-\Gamma_1} & e^{-i\phi(L)}\sqrt{1-\Gamma_1}\sqrt{1-\Gamma_2} \end{pmatrix}, \quad (5.5)$$

where the denominator Z_A has the form

$$Z_A = \sqrt{\Gamma_1(2-\Gamma_1)\Gamma_2(2-\Gamma_2)} \cosh[L_\alpha(q_A - q_{\text{peak}})]. \quad (5.6)$$

Here L_α is the effective propagation length (3.14), while q_{peak} is the transverse wave number defined by

$$q_{\text{peak}} = \frac{1}{2L_\alpha} \ln \left[\frac{\Gamma_1}{2-\Gamma_1} \frac{\Gamma_2}{2-\Gamma_2} \right]. \quad (5.7)$$

Both t_{ee} and t_{he} are peaked at $q_A = q_{\text{peak}}$. This peak momentum lies at the nodal point ($q_{\text{peak}} = 0$) only for ideal interfaces. In the presence of tunnel barriers the sign of q_{peak} is such that the order parameter has opposite sign at the two intersections of the line $q_A = q_{\text{peak}}$ with the Fermi surface.

Integration over q_A of electron current minus hole current gives the net (electrical) current,

$$I_2^A = G_0 V \frac{W}{2\pi} \int_{-\infty}^{\infty} dq_A [|(t_A)_{ee}|^2 - |(t_A)_{he}|^2] \\ = G_0 V \frac{W}{L} \frac{v_\alpha^2}{\pi v_F v_\Delta} \frac{1}{2-\Gamma_1} \frac{\Gamma_2}{2-\Gamma_2}. \quad (5.8)$$

Similarly, for the current through nodal point C we take the limit $q_A \rightarrow \infty$ of Eq. (4.6) and obtain the transmission matrix

$$t_C^\dagger = \frac{\sqrt{\Gamma_1\Gamma_2}}{e^{i\phi_\alpha(q_C)}Z_C} \times \begin{pmatrix} e^{i\phi(L)}\sqrt{1-\Gamma_1}\sqrt{1-\Gamma_2} & i\sqrt{1-\Gamma_1} \\ -ie^{i\phi(L)}\sqrt{1-\Gamma_2} & 1 \end{pmatrix}, \quad (5.9) \\ Z_C = \sqrt{\Gamma_1(2-\Gamma_1)\Gamma_2(2-\Gamma_2)} \cosh[L_\alpha(q_A + q_{\text{peak}})], \quad (5.10)$$

and then the current

$$I_2^C = -G_0 V \frac{W}{L} \frac{v_\alpha^2}{\pi v_F v_\Delta} \frac{1 - \Gamma_1}{2 - \Gamma_1} \frac{\Gamma_2}{2 - \Gamma_2}. \quad (5.11)$$

Note the minus sign in the formula for I_2^C . The current has opposite sign to that at nodal point A , since here holes rather than electrons tunnel across the system to contact 2.

The total current (per layer) through nodal points A and C becomes

$$I_2^A + I_2^C = G_0 V \frac{W}{L} \frac{v_\alpha^2}{\pi v_F v_\Delta} \frac{\Gamma_1}{2 - \Gamma_1} \frac{\Gamma_2}{2 - \Gamma_2}. \quad (5.12)$$

Comparison with Eq. (5.2) reveals that each tunnel barrier changes the sum of the current transmitted through a nodal point and the one opposite to it in momentum space, its time-reversed partner, by a factor of $\Gamma/(2 - \Gamma)$. As in the case of ideal NS contacts, the pair of nodal points B and D contribute a same amount, but with v_α replaced by $v_{\pi/2 - \alpha}$. The α -dependence again drops out of the total current $I_2 = I_2^A + I_2^B + I_2^C + I_2^D$. For the conductivity $\sigma = (I_2/V)(L/W)$ per layer we finally obtain

$$\sigma = \sigma_{\text{ideal}} \frac{\Gamma_1}{2 - \Gamma_1} \frac{\Gamma_2}{2 - \Gamma_2}. \quad (5.13)$$

VI. THERMAL CURRENT

The conductivity (5.13) vanishes in the weak tunneling limit $\Gamma_1, \Gamma_2 \rightarrow 0$, because the electron and hole contributions to the electrical current I_2 then become equal but of *opposite sign*. Electrons and holes contribute with the *same sign* to the thermal current,

$$I_{\text{thermal}} = L_0 G_0 T \delta T \frac{W}{2\pi} \int_{-\infty}^{\infty} dq [|t_{ee}|^2 + |t_{he}|^2], \quad (6.1)$$

with $L_0 = \pi^2 k_B^2 / 3e^2$ the Lorenz number. The thermal current flows from contact N_1 at temperature $T + \delta T$ into contact N_2 at temperature T . (Eq. (6.1) requires $\delta T \ll T$ and T sufficiently small that the transmission amplitudes may be evaluated at the Fermi energy $\varepsilon = 0$.)

We consider the (generic) case of misaligned nodes. Substitution of the expressions for t from Sec. VB, and summing over the pair of nodal points A and C , we find that

$$I_{\text{thermal}}^A + I_{\text{thermal}}^C = L_0 G_0 T \delta T \frac{W}{L} \frac{v_\alpha^2}{\pi v_F v_\Delta}. \quad (6.2)$$

Quite surprisingly, this turns out to be *independent of the tunnel probabilities* Γ_1 and Γ_2 . The total thermal current (per layer) also includes contributions from the nodal points B and D , and is – just as the electrical conductivity – independent of the angle α :

$$I_{\text{thermal}} = L_0 G_0 T \delta T \frac{W}{L} \frac{v_F^2 + v_\Delta^2}{\pi v_F v_\Delta}. \quad (6.3)$$

As discussed in Sec. VIII A, the thermal conductivity $\kappa = (I_{\text{thermal}}/\delta T)(L/W)$ extracted from Eq. (6.3) coincides with the bulk thermal conductivity of Ref. [22].

VII. SHOT NOISE

The zero-frequency noise power of time dependent electrical current fluctuations $\delta I_2(t)$ measured in contact number 2,

$$P_{22} = \int_{-\infty}^{\infty} dt \overline{\delta I_2(0) \delta I_2(t)}, \quad (7.1)$$

is given in terms of the transmission matrix elements by the general expression [30]

$$P_{22} = G_0 e V \frac{W}{2\pi} \int dq [|t_{ee}|^2 (1 - |t_{ee}|^2) + |t_{he}|^2 (1 - |t_{he}|^2) + 2 |t_{he}|^2 |t_{ee}|^2]. \quad (7.2)$$

As with the conductance, we work in the linear response regime, so the transmission matrix is to be evaluated at $\varepsilon = 0$.

We restrict ourselves to the case of misaligned nodes and substitute the expressions for t from Sec. VB. The integral over q contains four separate contributions, from q near nodes A , B , C , and D . The total result (per layer) is

$$P_{22} = G_0 e V \frac{W}{L} \frac{v_F^2 + v_\Delta^2}{\pi v_F v_\Delta} \times \frac{12(2 - \Gamma_1)^2(1 - \Gamma_2) + 8(1 - \Gamma_1)\Gamma_2^2 + \Gamma_1^2\Gamma_2^2}{3(2 - \Gamma_1)^2(2 - \Gamma_2)^2}. \quad (7.3)$$

The Fano Factor $F = P_{22}/eI_2$ is given by

$$F = \frac{12(2 - \Gamma_1)^2(1 - \Gamma_2) + 8(1 - \Gamma_1)\Gamma_2^2 + \Gamma_1^2\Gamma_2^2}{3\Gamma_1\Gamma_2(2 - \Gamma_1)(2 - \Gamma_2)}. \quad (7.4)$$

In the ideal limit $\Gamma_1, \Gamma_2 \rightarrow 1$ we find a Fano factor $F = 1/3$, three times smaller than the value $F = 1$ associated with a Poisson process. As discussed in the context of graphene [3, 14, 15], this is the same one-third reduction as in a diffusive metallic conductor and is a hallmark of pseudodiffusive transmission.

In the weak tunneling limit $\Gamma_1, \Gamma_2 \rightarrow 0$ the noise power remains finite,

$$\lim_{\Gamma_1, \Gamma_2 \rightarrow 0} P_{22} = G_0 e V \frac{W}{L} \frac{v_F^2 + v_\Delta^2}{\pi v_F v_\Delta}, \quad (7.5)$$

while the electrical current vanishes, $I_2 \propto \Gamma_1\Gamma_2 \rightarrow 0$. The electrical current fluctuations therefore become large relative to the time-averaged current in the presence of tunnel barriers. This is discussed in the context of resonant tunneling through midgap states in Sec. VIII B.

VIII. DISCUSSION

A. Comparison with bulk electrical and thermal conductivities

The electrical current I_2 and thermal current I_{thermal} that we have calculated describe transmission of electrons and holes over a finite length L of a clean d -wave superconductor. Earlier work [21, 22] calculated the electrical and thermal conductivities σ_0 and κ_0 of a disordered infinite system. These are in principle different systems, but we can still compare them by formally converting the currents through the finite system into bulk conductivities by means of $\sigma_0 \equiv (I_2/V)(L/W)$ and $\kappa_0 \equiv (I_{\text{thermal}}/\delta T)(L/W)$.

The thermal conductivity obtained in this way from the finite-system thermal current (6.3),

$$\kappa_0 = L_0 G_0 T \frac{v_F^2 + v_\Delta^2}{\pi v_F v_\Delta}, \quad (8.1)$$

is the same as the bulk thermal conductivity of Durst and Lee [22]. The results for the electrical conductivity differ, however. The bulk result [21, 22]

$$\sigma_0 = G_0 \frac{v_F}{\pi v_\Delta} \quad (8.2)$$

differs from the finite-system result (5.4) — even if we assume ideal NS interfaces. The difference between the factors v_F/v_Δ in Eq. (8.2) and $(v_F^2 + v_\Delta^2)/v_F v_\Delta$ in Eq. (5.4) is small in practice (because $v_F \gg v_\Delta$), but the difference does illustrate that these are different systems.

B. Interpretation in terms of resonant tunneling through midgap states

We have found that tunnel barriers at the NS interfaces reduce the transmitted electrical current, but not the thermal current nor the electrical noise. This result has a natural interpretation in terms of the midgap states at the NS interfaces. Midgap states are zero-energy edge states of the d -wave superconductor, which exist at momentum q along the edge if the order parameter has opposite sign at the two intersections of the line of constant q with the Fermi surface [28, 29]. The midgap states at the two NS interfaces have a small overlap, and therefore acquire a nonzero energy $\pm E_{\text{edge}}$ (tunnel splitting). Moreover, the coupling to the metal electrodes at $s = 0$, L introduces partial widths δE_0 , δE_L of the midgap states (tunnel broadening).

Tunneling through a pair of midgap states was studied in Ref. [31], in the context of Majorana bound states (which are a special type of nondegenerate midgap states). We can compare the transmission probabilities

resulting from that work,

$$|t_{ee}|^2 = |t_{eh}|^2 = |t_{he}|^2 = |t_{hh}|^2 = \frac{E_{\text{edge}}^2 \delta E_0 \delta E_F}{(E_{\text{edge}}^2 + \delta E_0 \delta E_L)^2}, \quad (8.3)$$

with the results from Sec. VB in the tunneling limit $\Gamma_1, \Gamma_2 \ll 1$,

$$|t_{ee}|^2 = |t_{eh}|^2 = |t_{he}|^2 = |t_{hh}|^2 = \frac{1}{4 \cosh^2[L_\alpha(q - q_{\text{peak}})]}. \quad (8.4)$$

We have defined

$$e^{L_\alpha q_{\text{peak}}} = \frac{1}{2} \sqrt{\Gamma_1 \Gamma_2}. \quad (8.5)$$

This comparison leads to the identification

$$\frac{E_{\text{edge}}}{\sqrt{\delta E_0 \delta E_L}} = \frac{2e^{L_\alpha q}}{\sqrt{\Gamma_1 \Gamma_2}}. \quad (8.6)$$

Resonant tunneling, with all transmission probabilities equal to $1/4$, occurs when $q = q_{\text{peak}}$, hence when $E_{\text{edge}} = \sqrt{\delta E_0 \delta E_L}$ (tunnel splitting of the midgap states equal to tunnel broadening). Because transmission from electron to electron and from electron to hole happens with the same probability (to leading order in Γ_1, Γ_2), the transmitted electrical current vanishes in the limit of small Γ . The thermal current I_{thermal} and electrical noise P_{22} remain finite, because $|t_{ee}|^2$ and $|t_{he}|^2$ contribute with the same sign to these quantities.

This interpretation explains the finite small- Γ limit for P_{22} and I_{thermal} , but it does not explain why the thermal current (6.3) turns out to be completely independent on the values of Γ_1 and Γ_2 . That remains a surprising result of our calculation, for which we have no qualitative explanation.

C. Outlook

We have shown how ballistic transport through a clean d -wave superconductor (such as single-crystal $\text{YBa}_2\text{Cu}_3\text{O}_{7-\epsilon}$) has features in common with graphene [1]: a pseudodiffusive $1/L$ scaling of the electrical current transmitted over a distance L , and a $1/3$ suppression of the electrical shot noise with respect to the Poisson value of uncorrelated current pulses. These effects have been observed in graphene [13–15] and it would be interesting to search for them in the high- T_c cuprates. The $1/L$ scaling should persist, with a modified slope, in the presence of tunnel barriers at the NS interfaces, and in the case of the thermal current we find that even the slope is independent of the tunnel barrier height.

There are more areas of correspondence between massless Dirac fermions in d -wave superconductors and in graphene, in addition to the pseudodiffusive transport studied in this work. We mention two such effects, as directions for future research.

- In graphene an electrostatic potential can displace the Fermi level away from the Dirac point of vanishing density of states. In the d -wave superconductor the supercurrent velocity \mathbf{v}_s enters into the Dirac equation (2.2) as a scalar term $\propto \sigma_0$ [32], and therefore has the same effect of displacing the Dirac point relative to the Fermi level. There is one curious difference with respect to graphene: the d -wave superconductor has two pairs of valleys and the Dirac point can be displaced independently in each pair (relative to the same Fermi level). With reference to Fig. 2, the component of \mathbf{v}_s in the x -direction acts on valleys at the nodal points A and C , while the component in the y -direction acts on those at B and D .
- While the role of an electrostatic potential in graphene is played by the supercurrent, an electric field in the d -wave superconductor plays the role of a magnetic field in graphene. If a sufficiently strong electric field could be induced in a thin-film cuprate superconductor, it might be possible to see effects analogous to the effects of Landau level quantization in graphene [33].

Acknowledgments

This research was supported by the Dutch Science Foundation NWO/FOM and by an ERC Advanced Investigator Grant.

APPENDIX A: NS INTERFACE MATRIX

In Sec. III B we derived the most general form of the transfer matrix of an NS interface, consistent with the requirement of particle flux conservation. The result in Eq. (3.6) has three undetermined parameters β_x , β_y , and β_z . Here we calculate the interface matrix by solving the Dirac equation in the interface layer and determine these unknown parameters. The interface layer is the region where the order parameter increases from 0 to its bulk value, over a healing length l_0 (which is typically of the same order of magnitude as the coherence length ξ_0).

As discussed in Ref. [34], in order to preserve Hermiticity, the Dirac equation (2.2) needs to be supplemented by terms containing the spatial derivatives of v_Δ :

$$-i[v_F\sigma_z\partial_x + v_\Delta\sigma_x\partial_y + (\partial_y v_\Delta)\sigma_x/2]\Psi = \varepsilon\Psi. \quad (\text{A1})$$

We assumed that the phase of Δ is constant, and set it to 0 (without loss of generality), thus v_Δ is real throughout, and is only a function of the distance s from the NS interface. An eigenstate $\Psi(s)$ of momentum q parallel to the NS interface satisfies

$$[-iJ\partial_s + J_1q - iv'_\Delta \sin(\alpha)\sigma_x/2]\Psi(s) = \varepsilon\Psi(s), \quad (\text{A2})$$

with the derivative of v_Δ denoted by the shorthand $v'_\Delta \equiv \partial_s v_\Delta$. Accordingly, the matrix \mathcal{A} in Eq. (2.8) becomes

s -dependent and gets a new term:

$$\mathcal{A}(s) = \mathcal{A}_0(s) - \frac{v'_\Delta(s) \sin \alpha}{2v_\alpha(s)^2} (\sigma_y v_F \cos \alpha - i v_\Delta(s) \sin \alpha). \quad (\text{A3})$$

Since $ql_0 v_F v_\Delta / v_\alpha^2 \simeq q/k_F \ll 1$ (in the relevant range of q 's near the nodal point), the integral of \mathcal{A}_0 over the interface layer is $\ll 1$ and may be neglected. Then $\mathcal{A}(s_1)$ commutes with $\mathcal{A}(s_2)$ for $0 < s_1, s_2 < l_0$, and therefore we can simply integrate Eq. (2.8) over the interface layer:

$$\begin{aligned} \mathcal{M}_{NS} &= \exp \left[i \int_0^{l_0} \mathcal{A}(s) ds \right] \\ &= \exp \left[\frac{-i}{2} \int_0^{\tan \theta} \frac{1}{1+u^2} (\sigma_y - iu) du \right] \\ &= \sqrt{\frac{v_F \cos \alpha}{v_\alpha}} \exp[-i\theta \sigma_y / 2], \end{aligned} \quad (\text{A4})$$

with $\theta = \arctan[(v_\Delta/v_F) \tan \alpha]$ as defined in Eq. (3.4). The result agrees with Eq. (3.6) with $\beta_x = \beta_y = \beta_z = 0$, and $v_N = v_F \cos \alpha$. The Fermi velocity mismatch contributes an additional factor $\sqrt{v_N/v_F}$ to the interface matrix, and in addition may cause internode scattering (as detailed in Sec. III C).

APPENDIX B: FULL SCATTERING MATRIX

In Secs. IV and V we have calculated the 2×2 transmission matrix t , which is the quantity we need for the transport properties considered. For reference, we give here the full 4×4 scattering matrix,

$$S = \begin{pmatrix} r & t' \\ t & r' \end{pmatrix}, \quad (\text{B1})$$

containing the 2×2 transmission matrices t (from left to right) and t' (from right to left), as well as the reflection matrices r (from left to left) and r' (from right to right). These matrices can be obtained from transfer matrix \mathcal{M} by constructing the four 2×2 sub-blocks X_{ij} ,

$$W\mathcal{M}W^\dagger = \begin{pmatrix} X_{11} & X_{12} \\ X_{21} & X_{22} \end{pmatrix}, \quad (\text{B2})$$

and then evaluating

$$\begin{aligned} r &= -X_{22}^{-1} X_{21}, & r' &= X_{12} X_{22}^{-1}, \\ t^\dagger &= X_{11}^{-1}, & t &= X_{22}^{-1}, \end{aligned} \quad (\text{B3})$$

cf. Eqs. (4.4) and (4.5).

We restrict ourselves to $\varepsilon = 0$ and misaligned nodes. Near node A we find the reflection matrices

$$r_A = \frac{1}{Z_A} \begin{pmatrix} -e^{L_\alpha q_A} \sqrt{1-\Gamma_1}(2-\Gamma_2) & -i\Gamma_1(e^{L_\alpha q_A} - \Gamma_2 \sinh L_\alpha q_A) \\ -i\Gamma_1(e^{L_\alpha q_A} - \Gamma_2 \cosh L_\alpha q_A) & -e^{L_\alpha q_A} \sqrt{1-\Gamma_1}(2-\Gamma_2) \end{pmatrix}, \quad (\text{B4})$$

$$r'_A = \frac{1}{Z_A} \begin{pmatrix} e^{-i\phi(L)} e^{L_\alpha q_A} \sqrt{1-\Gamma_2}(2-\Gamma_1) & -i\Gamma_2(e^{L_\alpha q_A} - \Gamma_1 \cosh L_\alpha q_A) \\ -i\Gamma_2(e^{L_\alpha q_A} - \Gamma_1 \sinh L_\alpha q_A) & e^{i\phi(L)} e^{L_\alpha q_A} \sqrt{1-\Gamma_2}(2-\Gamma_1) \end{pmatrix}. \quad (\text{B5})$$

The transmission matrix t_A is given by Eq. (5.5) and $t'_A = \sigma_y t_A^\dagger \sigma_y$. The resulting scattering matrix (B1) is unitary, $SS^\dagger = 1$, as it should be.

Similarly, near node C we find t_C given by Eq. (5.9), $t'_C = \sigma_y t_C^\dagger \sigma_y$, and the reflection matrices

$$r_C = \frac{1}{Z_C} \begin{pmatrix} -e^{-L_\alpha q_C} \sqrt{1-\Gamma_1}(2-\Gamma_2) & -i\Gamma_1(e^{-L_\alpha q_C} - \Gamma_2 \cosh L_\alpha q_C) \\ -i\Gamma_1(e^{-L_\alpha q_C} + \Gamma_2 \sinh L_\alpha q_C) & -e^{-L_\alpha q_C} \sqrt{1-\Gamma_1}(2-\Gamma_2) \end{pmatrix}, \quad (\text{B6})$$

$$r'_C = \frac{1}{Z_C} \begin{pmatrix} e^{-i\phi(L)} e^{-L_\alpha q_C} \sqrt{1-\Gamma_2}(2-\Gamma_1) & -i\Gamma_2(e^{-L_\alpha q_C} + \Gamma_1 \sinh L_\alpha q_C) \\ -i\Gamma_2(e^{-L_\alpha q_C} - \Gamma_1 \cosh L_\alpha q_C) & e^{i\phi(L)} e^{-L_\alpha q_C} \sqrt{1-\Gamma_2}(2-\Gamma_1) \end{pmatrix}. \quad (\text{B7})$$

APPENDIX C: CONDUCTANCE FOR ALIGNED NODAL POINTS

1. Alignment of nodes $A - C$.

For $|\alpha| \ll \xi_0/L$ the two nodal points A and C line up with the normal to the NS interface, while nodes B

and D remain misaligned. Restricting ourselves again to $\varepsilon = 0$, we may put $q_A = q_C = q$, $\phi_\alpha = 0$, $\mathcal{M}_A = \mathcal{M}_C$, and $L_\alpha = Lv_\Delta/v_F \equiv L_0$ in Eq. (4.6). The result is

$$t_{AC}^\dagger = \frac{(\Gamma_1 \Gamma_2)^{1/2}}{Z_{AC}} \begin{pmatrix} [1 + e^{2ik_F L} \sqrt{1-\Gamma_1} \sqrt{1-\Gamma_2}] \cosh L_0 q & i[\sqrt{1-\Gamma_1} + e^{-2ik_F L} \sqrt{1-\Gamma_2}] \sinh L_0 q \\ -i[\sqrt{1-\Gamma_1} + e^{2ik_F L} \sqrt{1-\Gamma_2}] \sinh L_0 q & [1 + e^{-2ik_F L} \sqrt{1-\Gamma_1} \sqrt{1-\Gamma_2}] \cosh L_0 q \end{pmatrix}, \quad (\text{C1})$$

$$Z_{AC} = 2\sqrt{1-\Gamma_1} \sqrt{1-\Gamma_2} \cos(2k_F L) + 2 - \Gamma_1 - \Gamma_2 + \Gamma_1 \Gamma_2 \cosh^2 L_0 q. \quad (\text{C2})$$

The current I_2^{AC} through the aligned nodes A and C follows from

$$I_2^{AC} = G_0 V \frac{W}{2\pi} \int_{-\infty}^{\infty} dq (|t_{ee}|^2 - |t_{he}^2|), \quad (\text{C3})$$

$$|t_{ee}|^2 - |t_{he}^2| = \frac{2\Gamma_1 \Gamma_2}{(2-\Gamma_1)(2-\Gamma_2) + 4\sqrt{1-\Gamma_1} \sqrt{1-\Gamma_2} \cos(2k_F L) + \Gamma_1 \Gamma_2 \cosh(2L_0 q)}. \quad (\text{C4})$$

For the total current I_2 we add the contribution from the (strongly) misaligned nodes B and D ,

$$I_2 = I_2^{AC} + G_0 V \frac{W}{L} \frac{v_\Delta}{\pi v_F} \frac{\Gamma_1}{2-\Gamma_1} \frac{\Gamma_2}{2-\Gamma_2}. \quad (\text{C5})$$

tunnel barriers,

$$I_2^{\min} = G_0 V \frac{W}{L} \frac{\Gamma^2}{\pi(2-\Gamma)^2} \left(\frac{v_F}{v_\Delta} \frac{\text{artanh } \chi}{\chi} + \frac{v_\Delta}{v_F} \right), \quad (\text{C6})$$

$$I_2^{\max} = G_0 V \frac{W}{L} \frac{1}{\pi} \left(\frac{v_F}{v_\Delta} + \frac{v_\Delta}{v_F} \frac{\Gamma^2}{(2-\Gamma)^2} \right), \quad (\text{C7})$$

As shown in Fig. 3, the current I_2 oscillates as a function of $k_F L$, between minima I_2^{\min} at $k_F L = 0 \pmod{\pi}$ and maxima I_2^{\max} at $k_F L = \pi/2 \pmod{\pi}$. (Similar oscillations were found in Ref. [25].) Simple expressions for these two values follow for the case $\Gamma_1 = \Gamma_2 \equiv \Gamma$ of equal

with abbreviation $\chi = 2(2-\Gamma)^{-1} \sqrt{1-\Gamma}$. For $\Gamma = 1$ we recover the ideal limit $I_2^{\min} = I_2^{\max} = \sigma_{\text{ideal}} VW/L$. For $\Gamma \ll 1$ we have instead $I_2^{\max} = G_0 V (W/\pi L) (v_F/v_\Delta)$, $I_2^{\min} = I_2^{\max} \times \frac{1}{4} \Gamma^2 |\ln \Gamma|$.

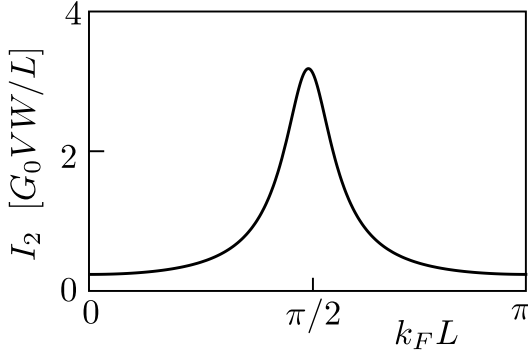


FIG. 3: Dependence on the separation L of the NS interfaces of the current I_2 into contact N_2 , for the interface orientation $\alpha = 0$ of aligned nodes A and C . Calculated from Eqs. (C3)–(C5) for parameters $\Gamma_1 = \Gamma_2 = 0.3$, $v_F/v_\Delta = 10$.

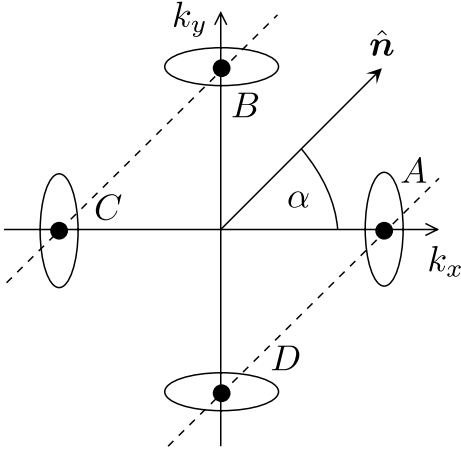


FIG. 4: Same as Fig. 2, but now for an angle $\alpha = \pi/4$ between the normal \hat{n} to the NS interface and the lines $x = 0$, $y = 0$ of vanishing order parameter. For this orientation the nodal points $A - D$ and $B - C$ are pairwise aligned with \hat{n} (dashed lines), so that they are pairwise coupled by a tunnel barrier at the interfaces.

2. Alignment of nodes $A - D$ and $B - C$

For $|\alpha - \pi/4| \ll \xi_0/L$, nodal points $A - D$ and $B - C$ are pairwise aligned with the normal to the NS interface (see Fig. 4). The transmission matrix t_{AD} through nodes $A - D$ is given by Eqs. (4.6) and (4.7) with \mathcal{M}_C replaced by \mathcal{M}_D . Similarly, for the transmission matrix t_{BC} through nodes $B - C$ we should replace \mathcal{M}_A by \mathcal{M}_B .

Considering first the transmission through nodes $A - D$, we see from Eq. (3.15) that $\mathcal{M}_D = \mathcal{M}_A^{-1}$ at $|\alpha| = \pi/4$, $q_A = q_D \equiv q$. Restricting ourselves to $\varepsilon = 0$, we find

$$t_{AD}^\dagger = \frac{2(\Gamma_1\Gamma_2)^{1/2}}{e^{i\phi_{\pi/4}(qA)}Z_{AD}} \begin{pmatrix} (1 + e^{i\psi(q)}\sqrt{1-\Gamma_1}\sqrt{1-\Gamma_2}) \cosh L_\alpha q & -ie^{-ik_FL\sqrt{2}}(\sqrt{1-\Gamma_2} - e^{i\psi(q)}\sqrt{1-\Gamma_1}) \sinh L_\alpha q \\ -i(e^{i\psi(q)}\sqrt{1-\Gamma_2} - \sqrt{1-\Gamma_1}) \sinh L_\alpha q & e^{-ik_FL\sqrt{2}}(e^{i\psi(q)} + \sqrt{1-\Gamma_1}\sqrt{1-\Gamma_2}) \cosh L_\alpha q \end{pmatrix}, \quad (\text{C8})$$

$$Z_{AD} = \Gamma_1\Gamma_2 + 4\sqrt{1-\Gamma_1}\sqrt{1-\Gamma_2} \cos \psi(q) + (2 - \Gamma_1)(2 - \Gamma_2) \cosh 2L_\alpha q, \quad (\text{C9})$$

with $L_\alpha = 2Lv_Fv_\Delta/(v_F^2 + v_\Delta^2)$ and the auxiliary function $\psi(q) = 2Lq(v_F^2 - v_\Delta^2)/(v_F^2 + v_\Delta^2) + k_FL\sqrt{2}$.

The current I_2^{AD} through the aligned nodes A and D follows from

$$I_2^{AD} = G_0V \frac{W}{2\pi} \int_{-\infty}^{\infty} dq (|t_{ee}|^2 - |t_{he}|^2), \quad (\text{C10})$$

$$|t_{ee}|^2 - |t_{he}|^2 = 2\Gamma_1\Gamma_2 \frac{(2 - \Gamma_1)(2 - \Gamma_2) + [\Gamma_1\Gamma_2 + 4\sqrt{1-\Gamma_1}\sqrt{1-\Gamma_2} \cos \psi(q)] \cosh(2L_\alpha q)}{[\Gamma_1\Gamma_2 + 4\sqrt{1-\Gamma_1}\sqrt{1-\Gamma_2} \cos \psi(q) + (2 - \Gamma_1)(2 - \Gamma_2) \cosh(2L_\alpha q)]^2}. \quad (\text{C11})$$

The contribution from the aligned nodes B and C is iden-

tical, so the total current becomes $I_2 = 2I_2^{AD}$.

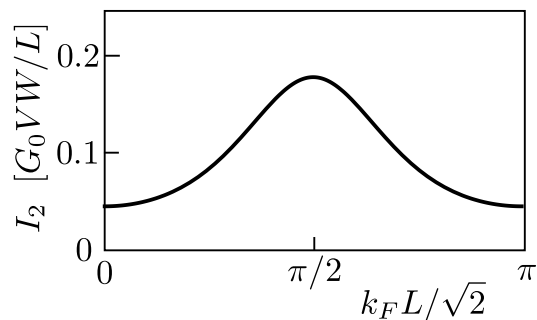


FIG. 5: Same as Fig. 3, but now for an interface orientation $\alpha = \pi/4$ of pairwise aligned nodes $A-D$ and $B-C$, calculated from Eq. (C10) for parameters $\Gamma_1 = \Gamma_2 = 0.3$, $v_F/v_\Delta = 10$.

For ideal interfaces ($\Gamma_1 = \Gamma_2 = 1$), we recover the result $I_2 = \sigma_{\text{ideal}} V W / L$. In the presence of tunnel barriers, I_2 again oscillates as a function of L , see Fig. 5.

-
- [1] C. W. J. Beenakker, Rev. Mod. Phys. **80**, 1337 (2008).
[2] M. I. Katsnelson, Eur. Phys. J. B **51**, 157 (2006).
[3] J. Tworzydło, B. Trauzettel, M. Titov, A. Rycerz, and C. W. J. Beenakker, Phys. Rev. Lett. **96**, 246802 (2006).
[4] A. R. Akhmerov and C. W. J. Beenakker, Phys. Rev. B **75**, 045426 (2007).
[5] E. Prada, P. San-Jose, B. Wunsch, and F. Guinea, Phys. Rev. B **75**, 113407 (2007).
[6] H. Schomerus, Phys. Rev. B **76**, 045433 (2007).
[7] Y. M. Blanter and I. Martin, Phys. Rev. B **76**, 155433 (2007).
[8] J. Cserti, A. Csordas, and G. David, Phys. Rev. Lett. **99**, 066802 (2007).
[9] A. Cresti, G. Grosso, and G. Pastori Parravicini, Phys. Rev. B **76**, 205433 (2007).
[10] M. Titov, EPL **79**, 17004 (2007).
[11] A. G. Moghaddam and M. Zareyan, Phys. Rev. B **79**, 073401 (2009).
[12] P. Dietl, G. Metalidis, D. Golubev, P. San-Jose, E. Prada, H. Schomerus, and G. Schön, Phys. Rev. B **79**, 195413 (2009).
[13] F. Miao, S. Wijeratne, Y. Zhang, U. C. Coskun, W. Bao, and C. N. Lau, Science **317**, 1530 (2007).
[14] L. DiCarlo, J. R. Williams, Y. Zhang, D. T. McClure, and C. M. Marcus, Phys. Rev. Lett. **100**, 156801 (2008).
[15] R. Danneau, F. Wu, M. F. Craciun, S. Russo, M. Y. Tomi, J. Salmilehto, A. F. Morpurgo, and P. J. Hakonen, Phys. Rev. Lett. **100**, 196802 (2008).
[16] R. A. Sepkhanov, Ya. B. Bazaliy, and C. W. J. Beenakker, Phys. Rev. A **75**, 063813 (2007).
[17] R. A. Sepkhanov and C. W. J. Beenakker, Opt. Commun. **281**, 5267 (2008).
[18] X. D. Zhang, Phys. Lett. A **372**, 3512 (2008).
[19] X. D. Zhang and Z. Y. Liu, Phys. Rev. Lett. **101**, 264303 (2008).
[20] D. J. van Harlingen, Rev. Mod. Phys. **67**, 515 (1995).
[21] P. A. Lee, Phys. Rev. Lett. **71**, 1887 (1993).
[22] A. C. Durst and P. A. Lee, Phys. Rev. B **62**, 1270 (2000).
[23] A. Altland, B. D. Simons, and M. R. Zirnbauer, Phys. Rep. **359**, 283 (2002).
[24] R. Harris, P. J. Turner, S. Kamal, A. R. Hosseini, P. Dosanjh, G. K. Mullins, J. S. Bobowski, C. P. Bidinosti, D. M. Broun, R. Liang, W. N. Hardy, and D. A. Bonn, Phys. Rev. B **74**, 104508 (2006).
[25] Z. C. Dong, Z. M. Zheng, and D. Y. Xing, J. Phys. Cond. Matt. **16**, 6099 (2004).
[26] S. Takahashi, T. Yamashita, and S. Maekawa, J. Phys. Chem. Sol. **67**, 325 (2006).
[27] W. J. Herrera, A. Levy Yeyati, and A. Martín-Rodero, Phys. Rev. B **79**, 014520 (2009).
[28] C.-R. Hu, Phys. Rev. Lett. **72**, 1526 (1994).
[29] S. Kashiwaya and Y. Tanaka, Rep. Prog. Phys. **63**, 1641 (2000).
[30] M. P. Anantram and S. Datta, Phys. Rev. B **53**, 16390 (1996).
[31] J. Nilsson, A. R. Akhmerov, and C. W. J. Beenakker, Phys. Rev. Lett. **101**, 120403 (2008).
[32] M. Franz and Z. Tešanović, Phys. Rev. Lett. **84**, 554 (2000).
[33] A. H. Castro Neto, F. Guinea, N. M. Peres, K. S. Novoselov, and A. K. Geim, Rev. Mod. Phys. **81**, 109 (2009).
[34] S. H. Simon and P. A. Lee, Phys. Rev. Lett. **78**, 1548 (1997).